Journal of Environmental Chemical Engineering 14 (2026) 120476

Contents lists available at ScienceDirect

Journal of Environmental Chemical Engineering

journal homepage: www.elsevier.com/locate/jece

Impact of granular fragment size on photogranulation systems: Reshaping wastewater treatment performance and microbial community ecology

Wei Chen [a,1], Qining Yu [a,1], Ji Li [b], Qiuyun Yang [a], Si Chen [c,e], Jiale Wang [d,*]

[a] Department of Water and Wastewater Engineering, Wuhan University of Science and Technology of Science and Technology, Wuhan 430065, China
[b] Department of Biotechnology, Delft University of Technology, van der Maasweg 9, Delft 2629 Hz, the Netherlands
[c] School of Resources and Environmental Science, Hubei University, Wuhan, Hubei Province 430062, China
[d] Hubei Key Laboratory of Multi-media Pollution Cooperative Control in Yangtze Basin, School of Environmental Science & Engineering, Huazhong University of Science and Technology (HUST), 1037 Luoyu Road, Wuhan, Hubei 430074, China
[e] Key Laboratory of Regional Development and Environmental Response, Wuhan, Hubei Province 430062, China

ARTICLE INFO

Keywords:
Photogranules
Re-granulation
Granular size
Microbial community dynamics
EPS
Biosynthesis

ABSTRACT

Photogranules are an emerging algal-bacterial system with potential for wastewater treatment and resource recovery. However, the mechanisms underlying their re-granulation after collapse remain poorly understood, limiting stable application. This study systematically examined the re-granulation mechanisms of photogranule fragments (0.3, 0.5 and 1.0 mm) by analysing growth dynamics, treatment performance, sludge characteristics and microbial community shifts. Results showed that 1.0-mm fragments (R3) achieved the average granular size of 3.34 ± 0.35 mm within 10 days of recovery, with 89.0 % ± 4.9 % chemical oxygen demand (COD) and 60.2 % ± 7.5 % TIN removal rates. In addition, Reactor 3 (R3) exhibited 50 % faster recovery rates and achieved a re-granulated particle size 33.07 % larger than that of smaller fragments. The extracellular polymeric substance (EPS) content in R3 was 273 mg/g VSS, with a protein (PN)/polysaccharide (PS) ratio of 4.7. In comparison, R1 and R2 showed lower Chl-a/Chl-b ratios and weaker EPS accumulation, consistent with their relatively lower pollutant removal efficiencies. Filamentous polysaccharides formed structural scaffolds enabling microbial colonization, reinforced by synergistic hydrophobic interactions and hydrogen bonding. Re-granulation drove microbial shifts from *Hyphomicrobium/Lysobacter* to functional genera *Methylobacillus*, *Chthonobacter*, and anammox bacterium *SM1A02*. These findings establish fragment size as a key control parameter in the re-granulation process, where robust EPS and functional microorganisms enable rapid re-granulation and high-efficiency nutrient removal. This study offers an in-depth understanding of photogranule stability and a novel strategy for sustainable wastewater treatment optimisation.

1. Introduction

Driven by rapid urbanization and global water scarcity, wastewater treatment plants are shifting toward multifunctional and sustainable solutions [1]. Aerobic granular sludge (AGS) has attracted attention for its compact structure, good settling ability, and high nutrient removal capacity [2,3], but it still suffers from excess sludge production and greenhouse gas (GHG) emissions [4,5]. Integrating algae with AGS provides a promising alternative to overcome these limitations. In algal-bacterial systems, photosynthetic algae supply oxygen and organic matter, while bacteria reciprocate by providing CO_2 and metabolites, forming a self-sustaining consortium that enhances treatment efficiency and stability [6-8]. Importantly, the additional biomass formed in such systems originates from photosynthetic growth rather than excess sludge accumulation [9], thereby reducing sludge disposal and improving resource recovery potential [10-12].

Photogranules represent an advanced form of such algal-bacterial systems [9]. With a low carbon footprint and algal-bacterial symbiosis, they exhibit enhanced structural stability and wastewater treatment performance [13], making them a promising alternative to conventional AGS. However, their stability is highly sensitive to factors such as organic loading rate [14], carbon-to-nitrogen (C/N) ratio [15], aeration intensity level [16], presence of toxicants, and temperature [17]. Granular size - typically ranging from sub-millimetre fragments to

* Corresponding author.
E-mail address: wangjiale19961124@gmail.com (J. Wang).
[1] The authors make the same contribution.

https://doi.org/10.1016/j.jece.2025.120476
Received 1 August 2025; Received in revised form 19 November 2025; Accepted 25 November 2025
Available online 29 November 2025

several millimetres [18] - and structural features such as pore density and size distribution affect substrate mass transfer and microbial succession, thereby influencing their stability [19,20]. For instance, nutrient diffusion limitations in larger cores can lead to disintegration [14]. Perturbations in these parameters can ultimately compromise granule integrity [21].

Granular disintegration is inevitable during the long-term operation of photogranules, which typically undergo repeated cycles of granulation, break-up, and re-granulation [22]. After break-up, photogranules form fragments of various sizes and some flocs; the flocs are washed out with the effluent, whereas the fragments remain in the reactor and regrow [22]. However, the influence of fragment size on the re-granulation process is still unclear, particularly in terms of its interactions with functional resilience and structural traits. Previous studies have shown that granule size affects dominant microbial taxa [23] and functional enzyme profiles, which in turn regulate system performance during re-granulation [24-26]. Therefore, investigating the role of fragment size in re-granulation is crucial for stabilizing and sustaining photogranule performance.

This study investigated the photogranule re-granulation by using different photogranule fragment sizes in lab-scale photo-sequencing batch reactors (PSBRs). The priority is to assess the effect of granular size on photogranule physicochemical properties. In parallel, pollutant removal efficiency was also evaluated to prove the efficiency and stability of the re-granulation system. Additionally, the structural dynamics were characterised via scanning electron microscopy (SEM) and confocal laser scanning microscopy (CLSM). Key functional microorganism shifts and their corresponding metabolic enzymes involved in re-granulation and nutrient removal were identified. By integrating the functional microalgae-bacteria synergy, spatial distribution, and surface functional group abundance within photogranules, this study provides new insights into the re-granulation of photogranules.

This study establishes theoretical foundations for practical photogranule 'disintegration-re-granulation' applications and proposes an innovative strategy for recycling photogranule fragments in wastewater treatment systems.

2. Materials and methods

2.1. Lab-scale reactor (PSBRs) set-up and operation

Mature photogranules had previously been cultivated in the laboratory [27], but they exhibited limited nutrient removal performance, possibly resulting from granule aging. To improve their re-granulation, these granules were collected and used in this study. Their settlement ability, measured as the sludge volume index after 5 min of settling (SVI_5) was 30 mL/g and an average granular size of 2.0 mm. The mature photogranules used for fragmentation were collected after long-term cultivation. Manual crushing was applied to obtain fragments with controlled size ranges (0.3, 0.5, and 1.0 mm), ensuring experimental reproducibility. Although this approach differs from spontaneous fragmentation, the resulting fragments retained comparable physicochemical and microbial features to those naturally disintegrated during operation. According to the different initial fragment sizes, the reactors were designated as R1 (0.3 mm), R2 (0.5 mm), and R3 (1.0 mm). The initial mixed liquor suspended solid (MLSS) and mixed liquor volatile suspended solid (MLVSS) concentrations were approximately 1500 and 1200 mg/L, respectively, across all PSBRs, with minor post-fragmentation reductions. The reactors were initiated at a lower MLSS (≈1.5 g/L), because flocculent biomass was largely washed out during decanting and only granular fragments are retained.

The experiment was conducted over 60 days using three laboratory-scale PSBRs. Each PSBR, constructed from acrylic columns (diameter: 6 cm; height: 100 cm), had a working volume of 2 L and was equipped with light-emitting diode strips with an intensity of 80 μmol/(m^2·s). The light was continuously irradiated throughout each operational cycle to maintain stable photosynthetic activity of the photogranules. The reactors were operated in 12 h cycles (HRT = 15 h) with a volume exchange ratio (VER) of 80 %, comprising 5 min of feeding, 705 min of aeration, 5 min of settling, and 5 min of effluent withdrawal. Continuous aeration was provided via an air pump through fine-bubble diffusers [28] at an airflow rate of 1.2 L/min, maintaining a dissolved oxygen concentration of 4 ± 1 mg/L. The PSBRs were operated at ambient temperature (25°C ± 5°C), and the pH was adjusted to 7.4 ± 0.5 using 1 mol/L HCl or $NaHCO_3$ solutions.

The influent wastewater used in this study was synthetic wastewater prepared in the laboratory. The initial water quality parameters were as follows: chemical oxygen demand (COD) = 600 ± 50 mg/L, methanol was chosen as the organic carbon source because it is a common external carbon source for denitrification [29]. Ammonium nitrogen (NH_4^+-N) = 40 ± 10 mg/L and nitrate nitrogen (NO_3^--N) = 20 ± 5 mg/L. NH_4^+-N and NO_3^--N were supplied by ammonium chloride (NH_4Cl) and potassium nitrate (KNO_3), respectively. In addition, Ca^{2+}, Mg^{2+}, and PO_4^{3-} were supplied by calcium chloride ($CaCl_2$, 10 mg/L), magnesium sulfate ($MgSO_4$, 10 mg/L), and potassium dihydrogen phosphate (KH_2PO_4, 10 mg/L), respectively. All reagents were of analytical grade and procured from Aladdin Industrial Corporation, China.

2.2. Reactors performance

COD, NH_4^+-N, NO_3^--N and NO_2^--N were analysed every 2 days using standard methods [30], and the SVI_5 and ML(V)SS concentrations were measured every 10 days. The chlorophyll content of the photogranules was determined following established protocols [31].

Loosely bound extracellular polymeric substances (LB-EPSs) and tightly bound extracellular polymeric substances (TB-EPSs) were extracted using a modified thermal extraction method [32]. Extracellular polymeric substance (EPS) contents and composition were quantified by analysing the major components: protein (PN) and polysaccharide (PS). PN was measured using the Lowry method [33], and PS was determined using a phenol-sulphuric acid assay [34].

2.3. Morphology observation of photogranules

For SEM observation, samples were fixed with 2.5 % glutaraldehyde at 4°C for 4 h, followed by dehydration through an ethanol gradient series (20 %, 40 %, 60 %, 80 % and 100 %, 15 min per step [35]. After dehydration, the samples were sputter-coated with gold before imaging.

For CLSM, photogranules were immobilised on glass slides, rinsed three times with phosphate-buffered saline (PBS, pH 7.4) and stained with protein-specific fluorophores (FITCs; Sigma, USA) for 10 min. After staining, PBS was used to remove excess dye, enabling the in situ visualisation of PS and PN distributions. Polysaccharides were differentiated using α-specific (ConA, Sigma, USA) and β-specific fluorescent probes (Calcofluor White, CW, Sigma, USA) [11]. Fluorescence signals were captured at excitation wavelengths of 543 nm (emission: 550–600 nm), 400 nm (emission: 410–480 nm) and 488 nm (emission: 500–540 nm) to distinguish α-polysaccharides, β-polysaccharides and proteins, respectively.

Excitation-emission matrix fluorescence spectroscopy was performed using a fluorescence spectrophotometer (F-7100 FL, Hitachi, Japan) equipped with a 1-cm quartz cuvette featuring four optical windows. The excitation (Ex) and emission (Em) slit widths were set to 5 nm at a scanning speed of 2400 nm/min. The Ex wavelengths ranged from 200 to 400 nm, whereas the Em wavelengths ranged from 250 to 500 nm. All fractionated samples were diluted 100-fold before analysis. To eliminate Raman scattering, background subtraction was performed using ultrapure water [36].

2.4. High-throughput sequencing

High-throughput sequencing was employed to analyse the diversity

of microbial community structures across the three PSBRs using samples collected before fragmentation (pre-fragmentation), after fragmentation (post-fragmentation) and at the end of the experiment. Sequencing was performed by Shanghai MajorBio Bio-pharm Technology Co., Ltd., China. The general workflow was as follows: DNA purity and concentration were assessed using a NanoDrop 2000 spectrophotometer (Thermo Fisher Scientific, USA). The qualified DNA extracts were subjected to polymerase chain reaction (PCR) amplification (ABI GeneAMP® 9700, Applied Biosystems, USA) using TransStart FastPfu DNA Polymerase (TransGen AP221–02, TransGen Biotech, Beijing) in a 20-μL reaction volume. The PCR conditions included initial denaturation at 95°C for 3 min, followed by 30 cycles of denaturation (95°C, 30 s), annealing (60°C, 30 s) and extension (72°C, 45 s), with a final elongation step at 72°C for 10 min. The amplified products were subjected to high-throughput sequencing on an Illumina MiSeq PE300 platform (Illumina, USA). Primer pairs targeting bacterial 16S rRNA (338 F: ACTCCTACGGGAGGCAGCAG; 806 R: GGACTACHVGGGTWTCTAAT) and eukaryotic 18S rRNA (528 F: GCGGTAATTCCAGCTCCAA; 706 R: AATCCRAGAATTTCACCTCT) were used. The sequencing data have been deposited in the NCBI Sequence Read Archive (SRA) under BioProject accession number PRJNA1335007. The functional gene abundances related to nitrogen metabolism, the TCA cycle, and other pathways were obtained through a predictive analysis based on 16S rRNA gene data using PICRUSt2 (Phylogenetic Investigation of Communities by Reconstruction of Unobserved States). The predicted KEGG Orthology (KO) functional profiles were normalized and visualized to illustrate the potential metabolic pathways within the microbial community.

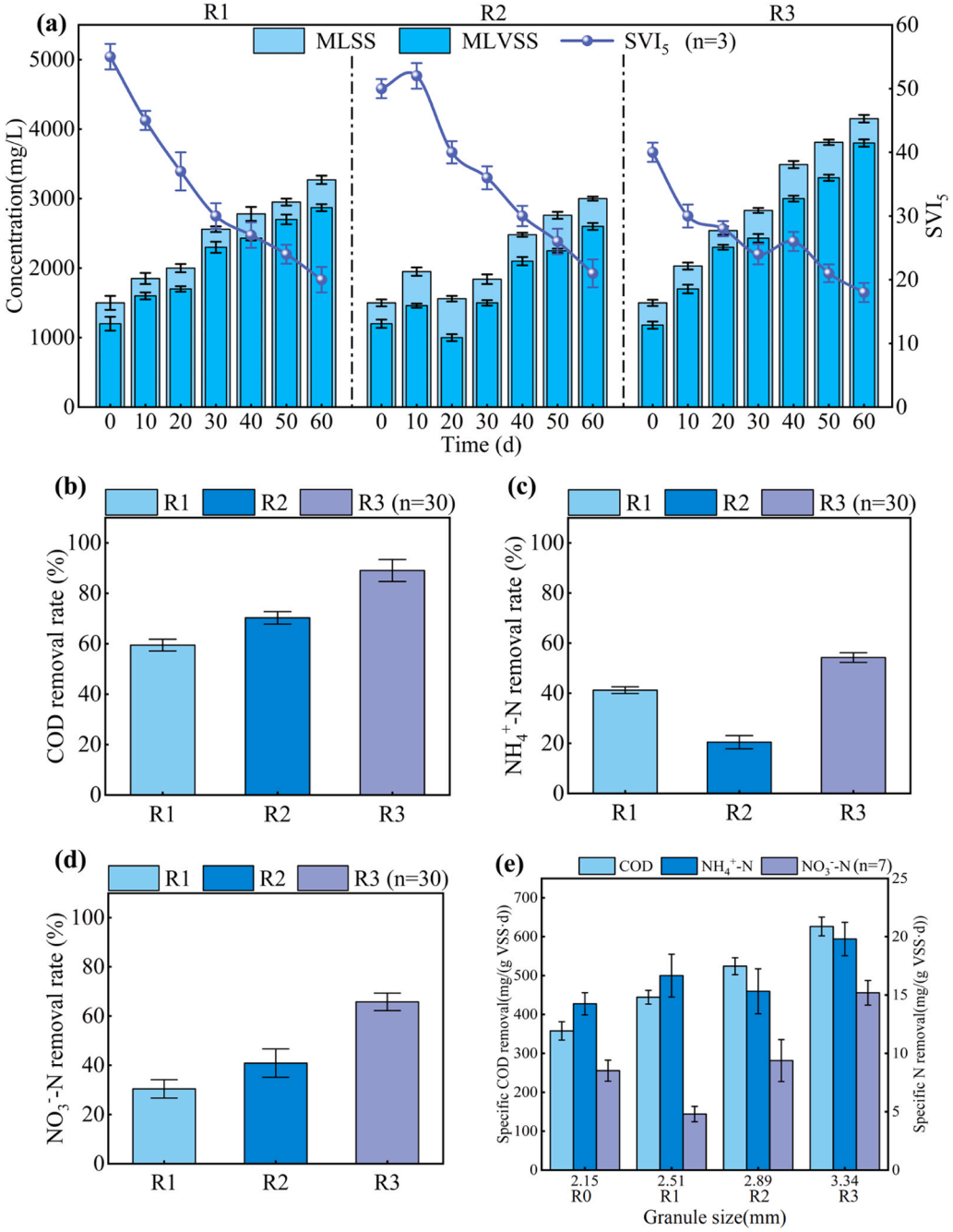

Fig. 1. MLSS, MLVSS and SVI_5 (a). Average removal efficiencies of COD (b), NH_4^+-N (c) and NO_3^--N (d) in the reactors (n = 30). COD, NH_4^+-N, and NO_3^--N removal rates at different granular sizes (the median particle diameter) at the end of the experiment (day 54–60) (e).

2.5. Statistical analysis

All measurements (e.g., COD, nitrogen species, EPS, chlorophyll) were performed in technical triplicates, and results are expressed as mean ± standard deviation. For high-throughput sequencing, replicate DNA extractions and sequencing depth were applied to minimize analytical bias. While the study was based on three 2 L SBRs without biological replicates due to sample and resource constraints, care was taken to maintain stable environmental conditions and repeated measurements to ensure reproducibility of observed trends.

3. Results

3.1. Reactors stability and performance

The initial MLSS and MLVSS concentrations were about 1500 and 1200 mg/L, and only minor reductions after fragmentation. As shown in Fig. 1(a), R1, R2 and R3 reached final concentrations of 3300, 3000 and 4200 mg/L, respectively. This result suggests that partial granule disintegration occurred in R2 during the early stage, leading to the release of fine flocs that were preferentially washed out with the effluent.

The initial SVI_5 values for R1, R2 and R3 were 55, 50 and 40 mL/g, respectively. R3 exhibited the lowest SVI_5 values, highlighting the influence of initial granular size on settling performance. All PSBRs showed progressive improvement in settling efficiency during re-granulation, with final SVI_5 values of 20, 21, and 18 mL/g for R1, R2, and R3, respectively-about 33 % lower than the pre-fragmentation value (30 mL/g). R3 was the lowest, but the differences among the three reactors were small, indicating that once mature, photogranules in all reactors achieved similarly good settling performance. Re-granulation from fragments enhanced the settling properties of photogranules, most likely due to structural densification.

Moreover, Fig. 1(b-d) shows the treatment performances of the three PSBRs, and all removal efficiencies were calculated based on the differences between influent and effluent concentrations. R3 achieved rapid and stable treatment performance within approximately 10 days, whereas R1 and R2 required about 15 days (Fig. S1). Recovery time was defined as the period needed to reach stable pollutant removal, indicating that R3 required approximately one-third less recovery time. The results demonstrate the critical influence of granular fragment size on the treatment efficiency and system stability. R3 demonstrated superior COD removal performance (89.0 % ± 4.9 %) (n = 30) compared with those of R1 (59.4 % ± 3.9 %) (n = 30) and R2 (70.3 % ± 3.6 %) (n = 30). R3 showed higher NH_4^+-N removal efficiency (54.2 % ± 3.7 %) (n = 30) than R1 (41.2 % ± 3.4 %) (n = 30) and R2 (20.5 % ± 12.8 %) (n = 30) (Fig. 1c). It also achieved the highest NO_3^--N removal (65.8 % ± 5.3 %) (n = 30), compared with R2 (40.9 % ± 14.2 %) (n = 30) and R1 (30.4 % ± 14.2 %) (n = 30). The large deviations, especially in R2, were due to early-stage fluctuations, while long-term data (Fig. S1) confirmed stable performance in the later phase. Superior nitrate removal in R3 may further be linked to larger anaerobic microzones within bigger granules, which provide niches for denitrifiers (Kedves et al., 2025). These observations collectively indicate that partial nitrification occurred simultaneously with heterotrophic and photoautotrophic denitrification. No NO_2^--N accumulation was detected.

The removal rates at the end of the experiment (54–60 d) were analyzed (Fig. 1e), with the median granule size used to reflect the overall trend between granule size and effluent indices, which helps minimize the influence of a few occasionally occurring extremely small or large granules. COD removal rates increased with photogranule size: R1 and R2 reached 444 ± 18 and 524 ± 22 mg-COD/(g VSS·d) (n = 7), respectively, while R3 achieved the highest rate of 626 ± 24 mg-COD/(g VSS·d) (n = 7), markedly higher than the pre-fragmentation value of 358 ± 24 mg-COD/(g VSS·d) (n = 7). These results suggest that larger initial fragments favoured COD removal. Meanwhile, NH_4^+-N and NO_3^--N removal rates fluctuated with granular size. R1 and R2 exhibited minimal improvement compared with that of the control (R0), even showing reduced performance in certain phases. However, R3 demonstrated consistent improvement: NH_4^+-N removal rate increased from 14 ± 1–20 ± 1 mg-N/(g VSS·d) (n = 7), and NO_3^--N removal rate increased from 9 ± 1–15 ± 1 mg-N/(g VSS·d) (n = 7). These findings collectively suggest that larger granular size is associated with enhanced metabolic activity in re-granulated photogranules.

3.2. Photogranule size distribution and morphology

Fig. 2a shows phase-contrast images of photogranules from different reactors. After crushing, fragmented photogranules exhibited sheet-like (thin, flat fragments) or flocculent (clustered) morphology. The average granular size before fragmentation was 2.15 mm. During the early stage of re-granulation, these fragments rapidly aggregated into clusters larger than their original size. Subsequently, newly formed small particles appeared, leading to a continuous increase in MLSS. This evolution suggests that the initial granulation process was dominated by fragment coalescence rather than gradual growth of individual particles. Only after 5-days operation, R3 exhibited initial granule formation, which subsequently evolved towards regular and smooth morphology. In contrast, R1 and R2 slowly formed cohesive granules after 10 days. By the end of the experiment, R1, R2 and R3 reached the final average sizes of 2.51 ± 0.15, 2.89 ± 0.21 and 3.34 ± 0.35 mm, respectively (Fig. 2c), indicating obvious granules growing and size-reframe.

The structures observation of photogranules by the SEM and CLSM were shown in Fig. 2b. Microscopically, structural evolution substantially varied among the PSBRs. In the initial phase, R1 exhibited rough surfaces and highly irregular morphologies, with filamentous bacteria serving as the structural backbone and numerous cocci attached to their surfaces. Finally, R1 transitioned to filamentous-dominated aggregates, in which bacilli replaced surface-adhered cocci. Regarding to R2, it primarily comprised intertwined filamentous bacteria with sparse bacilli and cocci attached superficial while cocci became the dominant microbial population, whereas residual filamentous structures persisted as skeletal frameworks after re-granulation. It should be noted that the process observed here represents re-granulation rather than the direct growth of intact small granules. The initial fragments exhibited irregular, sheet-like morphologies before cultivation (Fig. 2b), confirming their disintegrated state prior to structural reconstruction. In contrast, R3 maintained structural consistency throughout the experiment, with a filamentous bacterial scaffold that promoted stability and served as a framework for microbial colonization and nutrient retention, as also reported by Kedves and Kónya [37].

3.3. Sludge compositions and chemical characteristics

Chlorophyll-a (Chl-a) is the primary pigment capturing light energy and driving electron transport [38], while chlorophyll-b (Chl-b) functions as an accessory pigment that broadens the absorption spectrum and transfers excitation energy to Chl-a. Measuring both pigments therefore reveals not only the total photosynthetic capacity but also the light-harvesting strategy of the algal community [39-41]. In this study, the final Chl-a contents in R1 and R2 were 22 and 24 mg/g VSS, respectively, whereas R3 reached a much higher level of 34 mg/g VSS. Chl-b showed a similar trend, with R3 also exhibiting the highest concentration. These increases in absolute pigment contents indicate that larger fragments promoted faster algal proliferation and higher biomass accumulation. Beyond absolute values, the Chl-a/Chl-b ratio provides an indicator of algal photoacclimation: lower ratios reflect shade adaptation through broader spectral absorption, while higher ratios denote improved photosynthetic efficiency under stronger illumination. The calculated ratios were 3.62 (R1), 3.56 (R2), and 4.97 (R3), clearly demonstrating that R3 not only contained more pigments overall but also supported an algal community better adapted to light utilization.

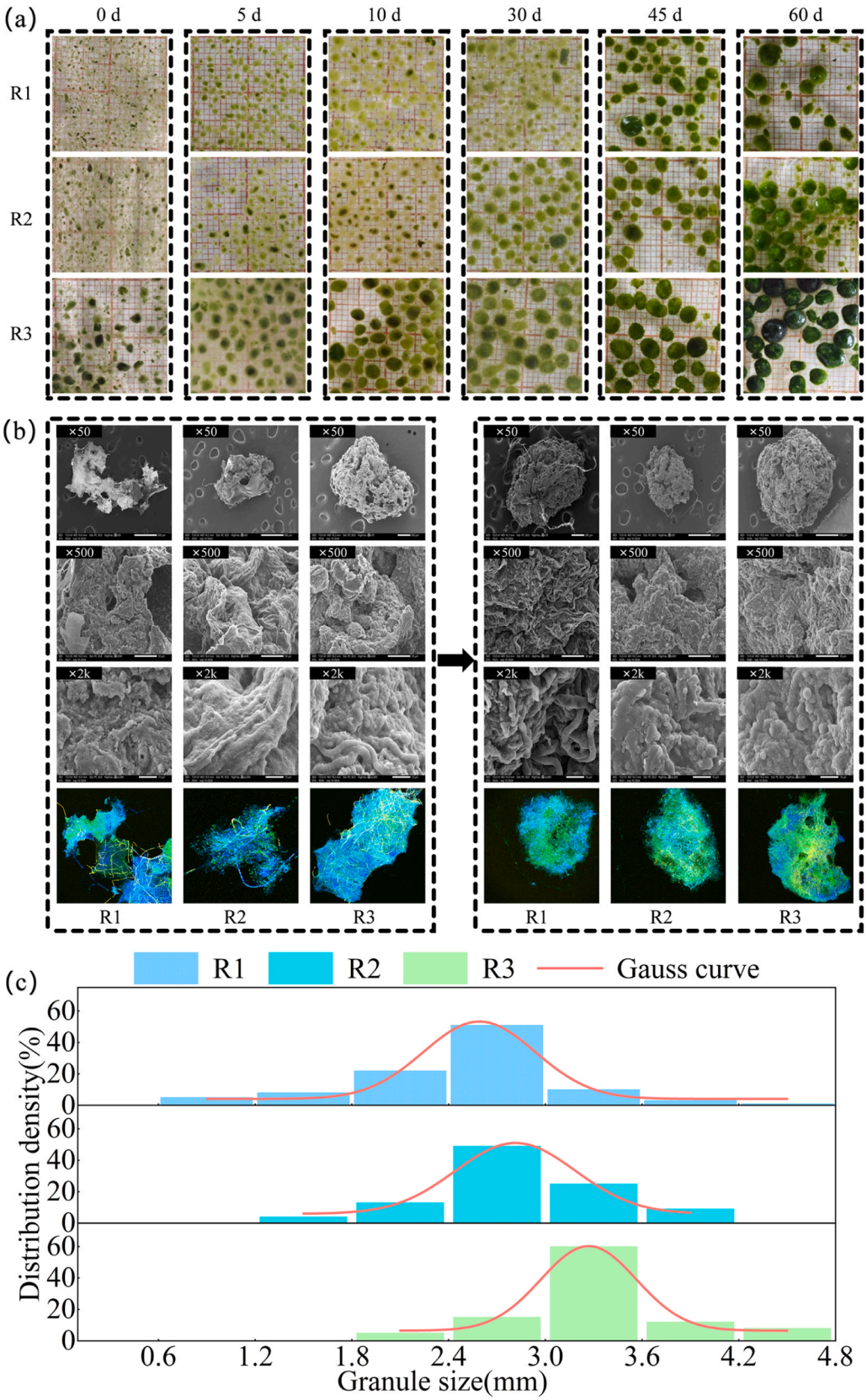

Fig. 2. Variation in the photogranule fragments in different reactors (a), SEM and CLSM images of photogranule fragments (b) and granular size distribution of photogranules after re-granulation (60 d) (c).

This simultaneous enhancement in pigment abundance and the Chl-a/Chl-b ratio explains the higher photosynthetic efficiency and pollutant removal observed in R3, in agreement with Pozzobon et al. [42].

During re-granulation, the EPS content increased across all reactors, with R3 showing the most pronounced accumulation. The final concentrations of protein (PN) in TB-EPS were 135 mg/g VSS in R1, 153 mg/g VSS in R2, and 225 mg/g VSS in R3. The total EPS concentrations were 179, 195, and 273 mg/g VSS, respectively, compared with a pre-fragmentation baseline of 150 mg/g VSS. These increases indicate that larger fragments promoted stronger EPS secretion. The PN/PS ratio also differed, being 3.1 in R1, 3.6 in R2, and 4.7 in R3, showing that R3 contained proportionally more proteins. Proteins in EPS enhance hydrophobic interactions, hydrogen bonding, and the formation of a cohesive gel-like matrix, thereby reinforcing microbial aggregation and granular stability [43]. In contrast, hydrophilic polysaccharides retain water within the matrix and improve its flexibility, supporting granule expansion during continuous collisions [44]. Higher polysaccharide levels promote stronger aggregation and structural growth, leading to larger and denser granules, which helps explain why R3 exhibited the largest particle size at the end of the experiment. The distinction between LB-EPS and TB-EPS further explains their complementary roles: LB-EPS interacts with external substrates, whereas TB-EPS provides mechanical support to maintain granule morphology. Thus, the higher EPS content and PN/PS ratio in R3 enhanced intercellular cohesion and structural integrity, leading to better settling and pollutant removal, consistent with previous findings [44-46].

The structures of photogranules were evaluated through the extraction and visualization of extracellular polymers (EPSs), which are involved in microbial activity and system stability [46]. This study divided EPSs into loosely bonded and tightly bonded EPS based on their bonding structures. LB-EPSs, which exhibit fibrous or flocculent morphologies, are distributed around cells with high specific surface areas, facilitating interactions with external substrates. In contrast, TB-EPSs provide direct structural support, maintaining cellular integrity and morphology [47]. As showed in Fig. S2, in all PSBRs, α-polysaccharides exhibited filamentous structures that diverged from their initial structures and formed an internal skeletal framework that facilitated microbial aggregation and granulation. By the end of the experiment, α-polysaccharides were uniformly distributed throughout the granules. This implied the enriched of filamentous microorganisms, which was observed by SEM (Fig. 2b). Similarly, β-polysaccharides and chlorophyll exhibited homogeneous spatial distributions in all PSBRs. In R1, proteins were predominantly localized in the outer layer of granules at the end of the experiments, whereas in R2, proteins accumulated in the granular core. Meanwhile, R3 exhibited an extensive protein distribution across both the inner and outer layers of granules. The spatial distributions of polysaccharides, proteins and chlorophyll in R3 were highly coordinated, forming a microporous network within the granule matrix. These interconnected pores facilitate substrate diffusion into the interiors of granules, thereby enhancing the metabolic exchange between microbial communities and their surrounding environments.

As shown in Fig. S3, tryptophan and tyrosine were identified as the dominant components in LB-EPSs and TB-EPSs, with tryptophan

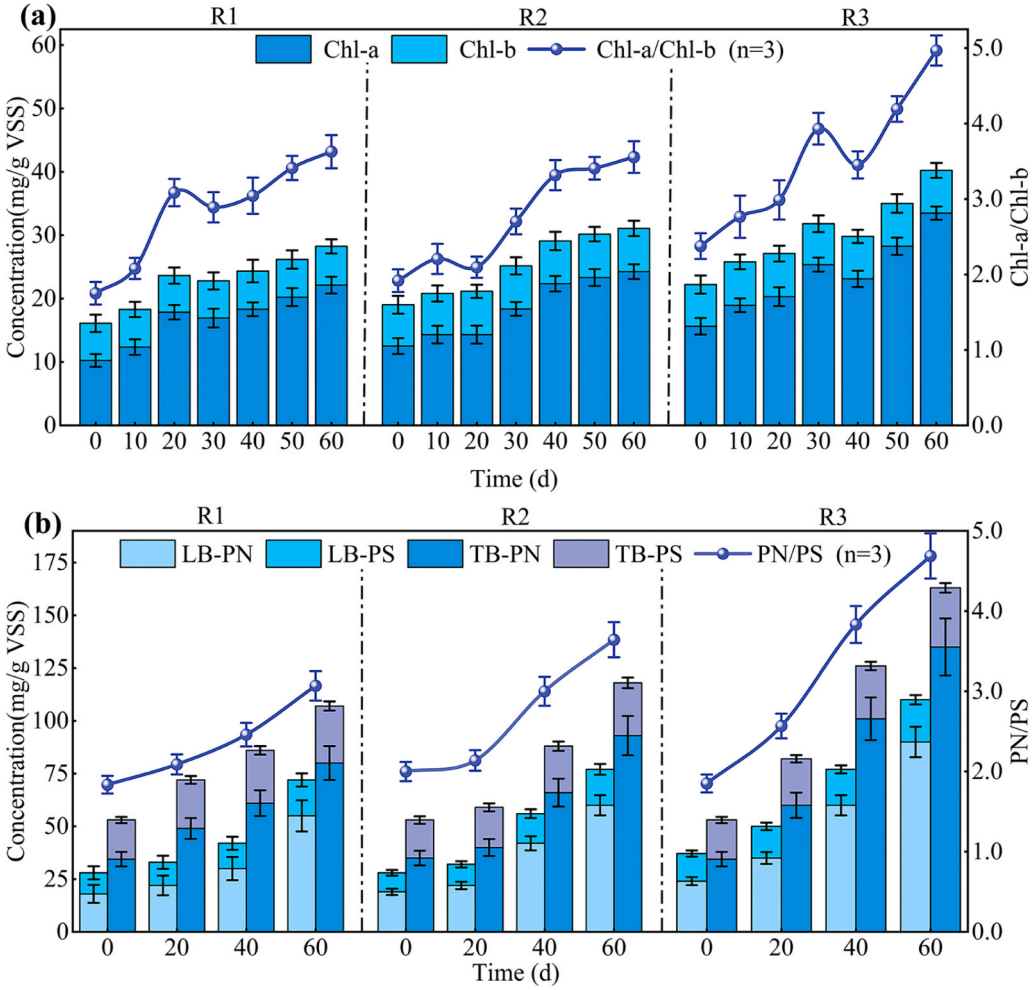

Fig. 3. Chlorophyll content and Chl-*a*/Chl-*b* ratio (a), EPS content and PN/PS ratio (b).

concentrations exceeding those of tyrosine. Both are synthesized via the shikimate pathway, which is widely conserved in bacteria, fungi, and algae [48,49]. Tryptophan, an essential amino acid for microbial growth, plays a critical role in intracellular protein synthesis, cellular proliferation and the maintenance of structural and functional integrity, with tyrosine further linked to pigment biosynthesis and photoprotection in algal cells [50,51]. In larger granules (R3), enhanced photosynthetic activity and higher microbial density promoted the synthesis of protein-like substances such as tryptophan and tyrosine, which supported cell proliferation, EPS secretion, and photoprotection. In contrast, smaller granules (R1 and R2) with weaker metabolic intensity produced less of these amino-acid-like fluorophores, resulting in slower re-granulation. Overall, EEM results indicate that tryptophan- and tyrosine-like substances are key components of the EPS that correlate with granule re-formation and size evolution.

3.4. Microbial community structure and metabolic pathway analysis

3.4.1. Microbial community analysis

Stichococcus (Chlorophyta) was dominant in R3, with a relative abundance of 59.1 %, far exceeding that in R1 (12.1 %) and R2 (14.4 %) (Fig. 4a). This genus forms short filaments and corresponds to the filamentous algae observed in SEM images, with its high abundance in R3 consistent with the SEM results (Fig. 2b). The increase in algal biomass was also associated with the higher chlorophyll content in R3 (Fig. 3b). Owing to its strong adaptability to environmental fluctuations [52], *Stichococcus* likely contributed to the greater resilience of R3 against the disturbances caused by granule disintegration and microbial exposure. *Auxenochlorella*, a spherical or oval alga, accounted for 9.9 %, 8.7 %, and 2.0 % in R1, R2, and R3, respectively. *Chlorella*, which shares a similar morphology, represented 5.7 %, 22.6 %, and 0.9 % in the same reactors. Both genera were enriched in R1 and R2, reflecting their preferential accumulation in these reactors (Fig. 2b). Notably, both *Chlorella* and *Auxenochlorella* have been reported to enhance pollutant removal efficiency [53].

As shown in Fig. S4, *Proteobacteria* dominated all PSBRs (R1:64.2 %, R2:69.9 %, R3:60.9 %), with *Bacteroidota*, *Planctomycetota*, and *Cyanobacteria* as subdominant phyla. *Planctomycetota* have been reported to exhibit hydrolytic potential for complex polysaccharide degradation [54], whereas *Proteobacteria* and *Bacteroidota* are linked to sludge

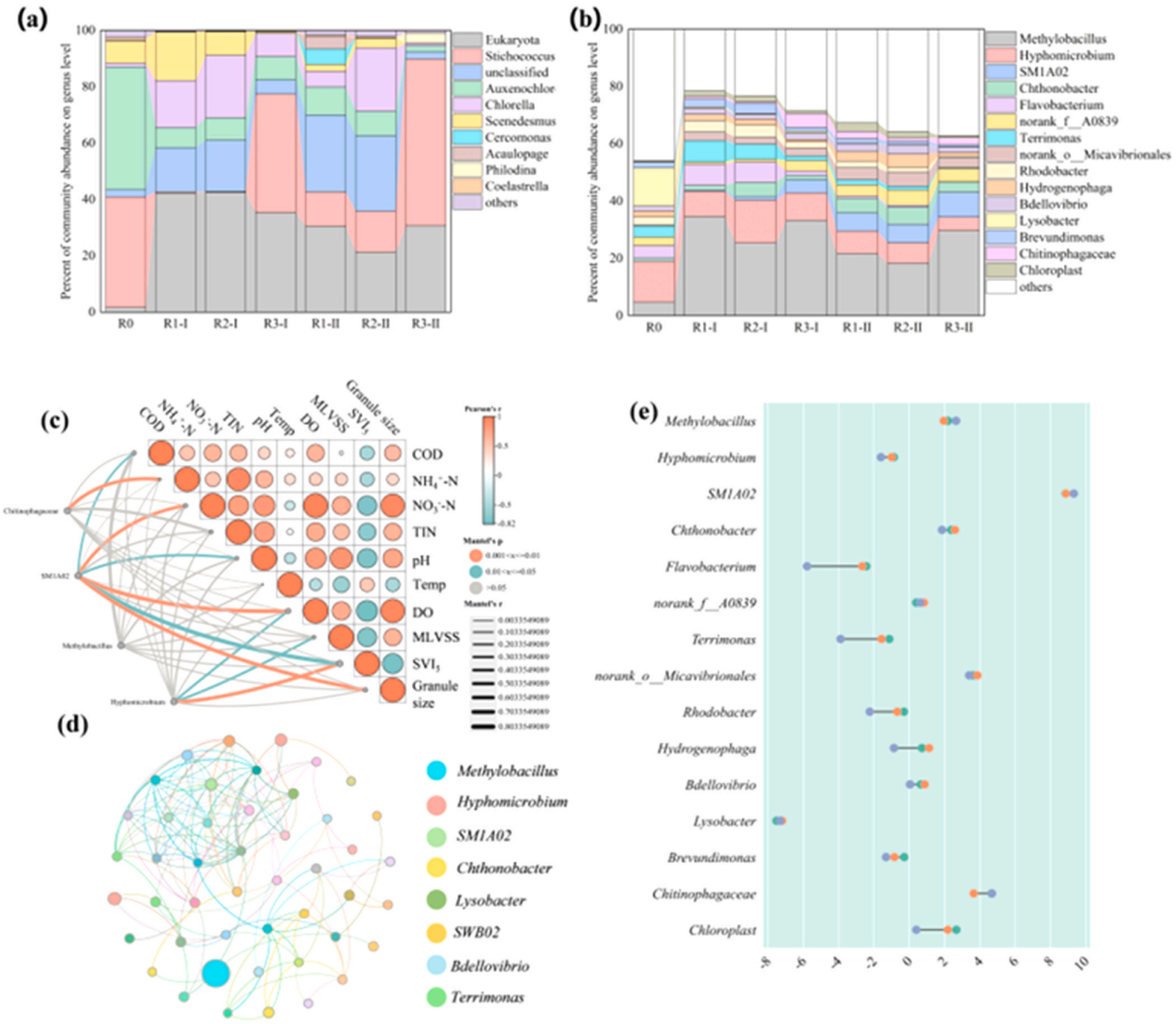

Fig. 4. Relative abundance of eukaryotes at the genus level (a), Relative abundance of bacteria at the genus level (b), environmental factor analysis (c), network analysis of microbial taxa correlations (d) and bacterial dumbbell plot at the genus level (e).

aggregation, EPS secretion, and nutrient removal [55]. At genus level (Fig. 4b), R3 exhibited a substantially higher abundance of the anammox bacterium *SM1A02* [56] (8.7 %) compared to R1 (6.3 %) and R2 (6.4 %), likely facilitated by micro-anaerobic zones within larger granules, which enhanced anaerobic ammonium oxidation and ammonia removal efficiency [57]. Concurrently, *Methylobacillus* (an obligate methylotroph) [58] increased in all reactors, peaking in R3 (29.7 %) (R1: 21.7 %, R2: 18.3 %), and its role as a core node of the network (Fig. 4d) is critical for maintaining community stability. In contrast, *Hyphomicrobium* declined, likely because granule fragmentation exposed microorganisms to the aqueous environment, which was unsuitable for its survival [59]. *Chthonobacter* abundance increased in all PSBRs and was correlated with denitrification activity and biofilm stability [60]. As shown in Fig. 4(c, e), these genera (*Chthonobacter*, *SM1A02*) were considerably enriched in R3 and exhibited strong associations with COD, ammonia and nitrate removal efficiencies as well as photogranule granular size and settleability. Overall, the microbial community during re-granulation approached the mature photogranule profile yet differed from any single initial size group, implying that new granules formed through fragment integration rather than single-fragment growth. Larger granule fragments post-regranulation facilitated the enrichment of functionally critical microbial communities, which directly enhanced the treatment performance of regenerated photogranules through synergistic substrate utilization and metabolic coordination.

3.4.2. Metabolic pathways

To further elucidate the mechanism by which granular size facilitates photogranule formation, we investigated the pathways of nitrogen metabolism, porphyrin metabolism, and the tricarboxylic acid (TCA) cycle, along with changes in the abundance of associated enzymes, referencing previous findings [61].

In algal-bacterial systems, nitrogen removal relies on bacterial nitrification/denitrification and algal assimilation [62]. Crucially, the higher abundances of denitrification-related enzymes (*narG, nirK*, *nrfA*, and *nirB*) in R3 contributed to its superior nitrate removal performance. The abundance of denitrifying enzymes in R1 was lower than in R0, which aligns with its reduced nitrate removal rate relative to R0. Conversely, elevated *Hao* in R1 and R2 indicated

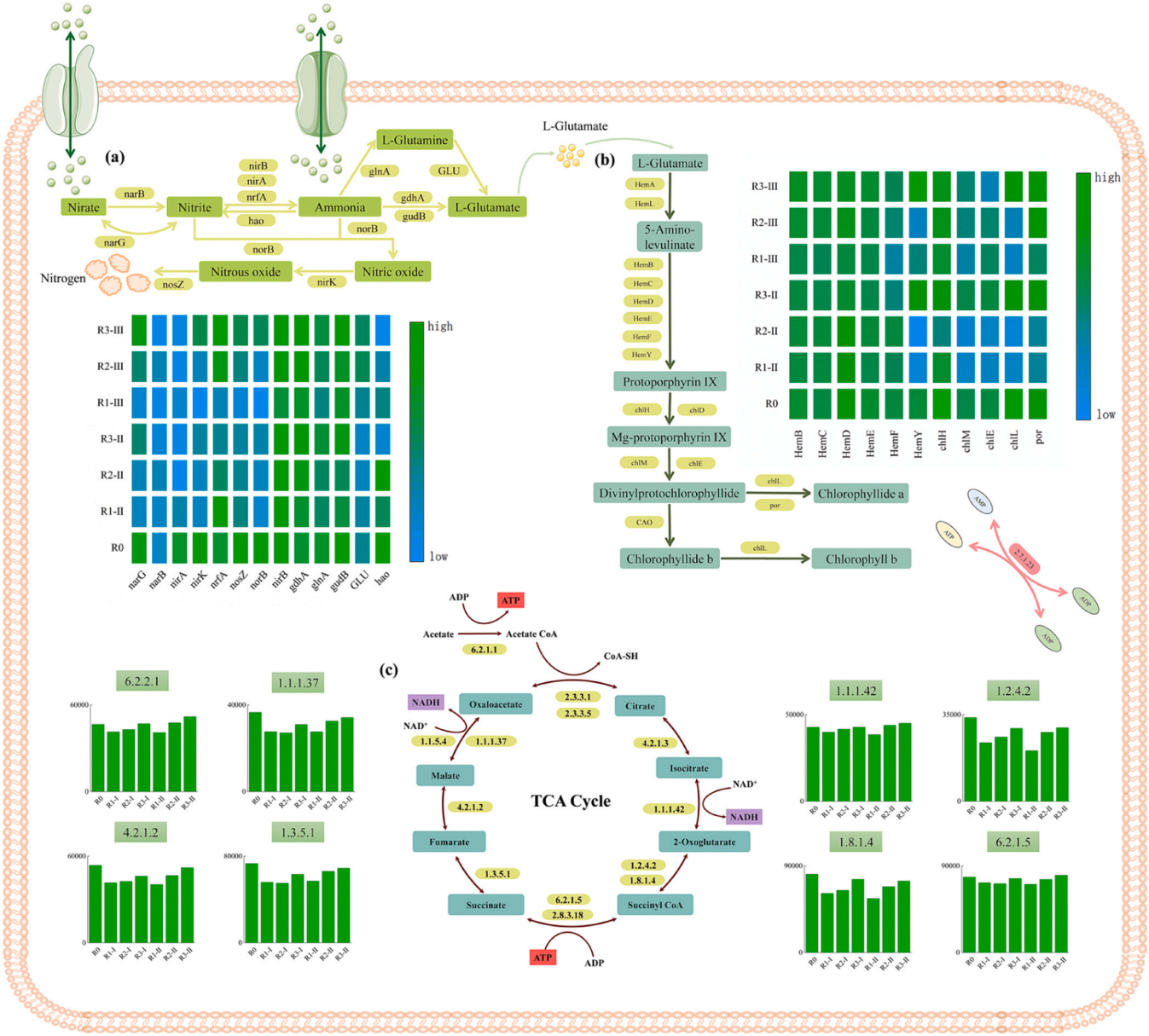

Fig. 5. Nitrogen metabolism (a), porphyrin metabolism (b), and TCA cycle pathways (c), along with the relative abundances of key associated enzymes.

nitrification-dominated ammonia conversion to nitrite. Furthermore, R3's enriched *gdhA* and *GLU* enhanced ammonium assimilation into glutamate, stimulating TCA cycle activity and metabolic flux. Although nitrogen pathways (nitrification, denitrification, anammox) were consistent across reactors, divergent enzyme abundances drove performance disparities, directly linking granule fragment size to enzymatic potential and treatment performance.

The TCA cycle serves as a critical pathway for carbohydrate metabolism and microbial energy production [63]. As shown in Fig. 5c, genes encoding TCA cycle enzymes exhibited fragment-size-dependent regulation: Acetyl-CoA synthetase (EC 6.2.1.1) abundance was highest in R3 and lowest in R1, indicating enhanced acetate entry into the TCA cycle. Furthermore, R3 showed elevated abundances of oxoglutarate dehydrogenase (EC 1.2.4.2), malate dehydrogenase (EC 1.1.1.37), and succinate dehydrogenase (EC 1.3.5.1) compared to pre-disintegration levels. This enzymatic upregulation enabled larger granules to metabolize more organic substrates, stimulating EPS secretion and establishing a self-reinforcing feedback loop that enhanced granule stability, regranulation rate, and overall system performance.

Porphyrin metabolism is intrinsically linked to chlorophyll synthesis [64]. Genes encoding enzymes involved in the L-glutamate-to-protoporphyrin IX pathway-*hemC*, *hemB*, *hemE*, *hemF* and *hemY*-were upregulated in R3 but downregulated in R1 and R2. The elevated abundances of these enzymes ensured enhanced chlorophyll synthesis in R3, consistent with the results shown in Fig. 3b. The increased chlorophyll production in R3 facilitated efficient material and energy exchange between algae and bacteria within the granules, thereby improving granule stability.

4. Discussion

4.1. how size influence re-granulation

Fragment size critically dictated photogranule re-granulation efficacy through synergistic compositional, structural, and microbial cascades (Fig. 6). Larger fragments (1.0 mm) retained superior EPS reserves-notably elevated PN content and PN/PS ratios-which enhanced hydrophobicity and stability, accelerating dense structural reassembly and ensuring exceptional settleability (e.g., low SVI_5). Structurally, these fragments preserved a structural "memory" that facilitated rapid microbial colonization, while their filamentous α-polysaccharide networks (CLSM-verified) formed skeletal frameworks for bacterial adhesion and nutrient retention. Microbially, size governed algal assembly: R3's dominance of filamentous *Stichococcus* (59.1 %) generated intertwined α-polysaccharide matrices that anchored bacteria and enabled metabolic reciprocity - algae supplied photosynthetic oxygen/organics to bacteria, which reciprocated with organic acids to sustain the algal framework. This shift from *Chlorella* to *Stichococcus* dominance may be attributed to the latter's stronger attachment ability and higher tolerance to limited oxygen and light diffusion, allowing it to maintain

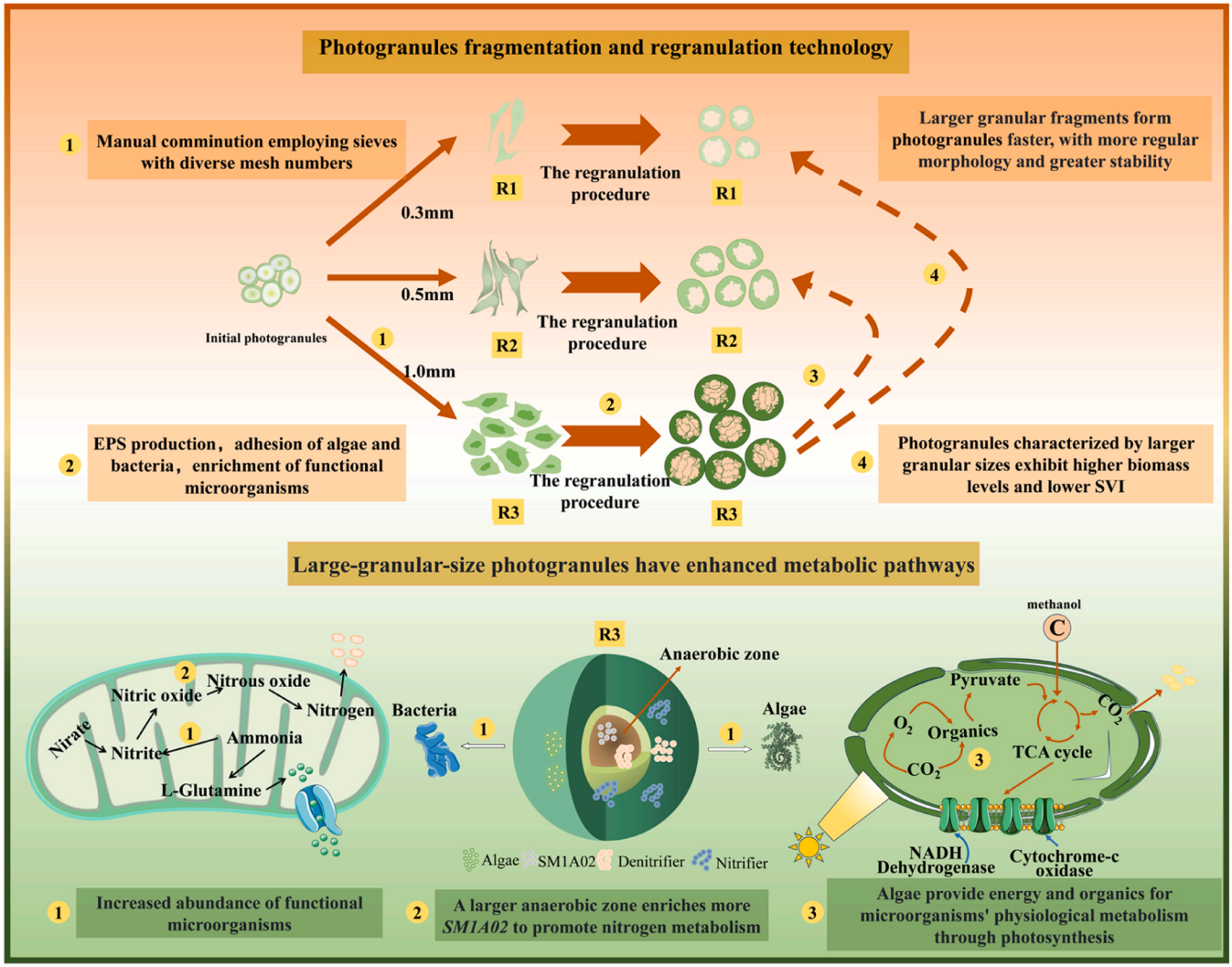

Fig. 6. Schematic of photogranule disintegration–re-granulation and granular size effects on metabolic pathways.

structural stability within large granules. In contrast, the Chlorella-driven systems of R1 and R2 produced homogeneous β-polysaccharides, lacking cohesive architecture. This underpinned R3's faster wastewater treatment recovery, as higher chlorophyll levels optimized photosynthetic efficiency, energizing bacterial metabolism while PN-mediated aggregation reinforced granular integrity. The enrichment of *Methylobacillus* and *SM1A02* indicates a synergistic interaction between methylotrophic denitrification and anammox. Compared with mixed-carbon-source wastewaters, methanol as a single carbon source selectively enriched *Methylobacillus*, which coupled methanol oxidation with nitrate reduction to supply nitrite for *SM1A02*, thereby enhancing overall nitrogen removal efficiency. However, identification based solely on 16S rRNA sequencing cannot confirm the metabolic activity of anammox bacteria; therefore, their performance was not analyzed in this study. To address this limitation, future work will employ metagenomic and metatranscriptomic approaches to elucidate the potential roles of anammox bacteria and their interactions with algal-bacterial consortia during the re-granulation process. Consequently, the filamentous framework in larger fragments structured a hierarchical microbial habitat, in which microalgae provided O_2 and organic matter through photosynthesis, while bacteria supplied CO_2 and nutrients that promoted algal growth [10,24,23,25]. This reciprocal interaction enhanced structural stability and facilitated simultaneous carbon and nitrogen removal, ultimately demonstrating that fragment size inherently encodes regeneration advantages through physicochemical-metabolic interactions.

4.2. Promising strategy to promote disintegration-re-granulation

Unlike conventional re-granulation strategies-such as polyaluminium chloride addition [65], Ca^{2+} supplementation [66], zero-valent iron enhancement [54] and functional microbe inoculation [67] - this study proposes a size-dependent operational strategy for photogranule systems. The proposed strategy aims to balance treatment performance and system stability by optimizing the initial granule size and biomass concentration, thereby mitigating the risks of chemical residues and bio-competitive inhibition associated with external additives. For example, while Ca^{2+} addition can accelerate granulation, excessive concentrations (>200 mg/L) may inhibit nitrifier activity and lead to colonization failure of bioaugmented strains (e.g., *Nitrosomonas*), causing fluctuations in denitrification efficiency (± 15 %). In contrast, the re-granulation observed in our study proceeded spontaneously, driven by the intrinsic algal-bacterial interactions within the photogranules. Photogranules leverage synergistic interactions between algal photosynthetic oxygen supply and bacterial metabolic feedback to dynamically reconfigure EPS networks (23 % increase in polysaccharides), enabling low-cost, ecologically benign regeneration. Notably, functional microbial shifts during re-granulation lead to divergent performance outcomes: larger initial fragments exhibit enhanced treatment efficacy, whereas smaller fragments exhibit underperformance. This particle-size-dependent divergence highlights the need for strategies to homogenise post-disintegration system performance, such as optimising key operational parameters (e.g., dissolved oxygen concentration, C/N ratio, and hydraulic retention time) and developing particle-size-selective approaches (e.g., screening and reassembling larger fragments to accelerate re-granulation). In engineering practice, resolving the performance heterogeneity due to post-disintegration granular size divergence will become a key research direction for the long-term stable application of photogranule technology.

5. Conclusions

This study establishes a fragment size-driven photogranule re-granulation strategy that enables rapid structural recovery and enhanced wastewater treatment without chemical additives. Critically, 1.0-mm fragments regenerated 50 % faster (within 10 days) and formed 33 % larger granules than smaller counterparts by leveraging inherent structural retention (e.g., preserved PN/PS ratios) to create stable microenvironments. Improved mass transfer accelerated microbial nutrient assimilation and proliferation, facilitating synergistic advantages: enriched anammox bacteria (*SM1A02*) optimized ammonium oxidation; glutamate-mediated EPS biosynthesis (via glutamine synthetase, EC 6.3.1.2) reinforced granular stability; and elevated algal biomass intensified photosynthetic substrate supply for bacterial metabolism. Consequently, regenerated granules achieved superior structural integrity and treatment performance - exceeding pre-fragmentation levels (50 % COD and 30 % TIN removal) with 90 % COD and 60 % TIN removal-thus providing a theoretical foundation for sustainable photogranule reactor optimization.

CRediT authorship contribution statement

Jiale Wang: Writing – review & editing, Writing – original draft, Supervision, Conceptualization. **Si Chen:** Visualization, Formal analysis. **Qining Yu:** Writing – review & editing, Writing – original draft, Validation, Investigation. **Wei Chen:** Writing – review & editing, Funding acquisition, Formal analysis, Data curation. **Qiuyun Yang:** Writing – review & editing, Visualization, Validation. **Ji Li:** Validation, Formal analysis, Data curation.

Declaration of Competing Interest

The authors declare the following financial interests/personal relationships which may be considered as potential competing interests: We declare that we have no financial and personal relationships with other people or organizations that can inappropriately influence our work. Also, there is no professional or other personal interest of any nature or kind in any product, service and /or company that could be construed as influencing the position presented in, or the review of, the manuscript entitled.

Acknowledgements

The work was financially supported by the Fundamental Research Funds for the Central Universities (YCJJ20252316). The research was conducted on the Public Service Platform of Environmental Research Facilities within the School of Environmental Science and Engineering at Huazhong University of Science and Technology. In addition, we acknowledge support of the Huazhong University of Science & Technology Analytical & Testing Center.

Appendix A. Supporting information

Supplementary data associated with this article can be found in the online version at doi:10.1016/j.jece.2025.120476.

Data availability

Data will be made available on request.

References

[1] N.T. Bahgat, P. Wilfert, L. Korving, M. van Loosdrecht, Integrated resource recovery from aerobic granular sludge plants, Water Res. 234 (2023) 119819.
[2] Y. Nancharaiah, G.K.K. Reddy, Aerobic granular sludge technology: mechanisms of granulation and biotechnological applications, Bioresour. Technol. 247 (2018) 1128–1143.
[3] M. Pronk, M. De Kreuk, B. De Bruin, P. Kamminga, Rv Kleerebezem, M. Van Loosdrecht, Full scale performance of the aerobic granular sludge process for sewage treatment, Water Res. 84 (2015) 207–217.
[4] M.B. Shahabadi, L. Yerushalmi, F. Haghighat, Impact of process design on greenhouse gas (GHG) generation by wastewater treatment plants, Water Res. 43 (10) (2009) 2679–2687.

[5] M. Zhang, J. Gu, Y. Liu, Engineering feasibility, economic viability and environmental sustainability of energy recovery from nitrous oxide in biological wastewater treatment plant, Bioresour. Technol. 282 (2019) 514–519.
[6] R. Cheng, D. Huang, X. Xu, F. Yang, Optimal algae species inoculation strategy for algal-bacterial granular sludge: sludge characteristics, performance and microbial community, J. Environ. Manag. 370 (2024) 123011.
[7] J. Marchand, P. Heydarizadeh, B. Schoefs, C. Spetea, Ion and metabolite transport in the chloroplast of algae: lessons from land plants, Cell. Mol. Life Sci. 75 (12) (2018) 2153–2176.
[8] M.J. Torres, C.M. Bellido-Pedraza, A. Llamas, Applications of the microalgae chlamydomonas and its bacterial consortia in detoxification and bioproduction, Life 14 (8) (2024) 940.
[9] C. Billery, G. Gaval, J. Hamelin, K. Milferstedt, Phototrophic aggregates for wastewater treatment: identifying key parameters for formation and characterization, Rev. Environ. Sci. Bio/Technol. (2025) 1–26.
[10] A.S. Abouhend, A. McNair, W.C. Kuo-Dahab, C. Watt, C.S. Butler, K. Milferstedt, J. Hamelin, J. Seo, G.J. Gikonyo, K.M. El-Moselhy, The oxygenic photogranule process for aeration-free wastewater treatment, Environ. Sci. Technol. 52 (6) (2018) 3503–3511.
[11] L.M. Trebuch, O.M. Bourceau, S.M. Vaessen, T.R. Neu, M. Janssen, D. de Beer, L. E. Vet, R.H. Wijffels, T.V. Fernandes, High resolution functional analysis and community structure of photogranules, ISME J. 17 (6) (2023) 870–879.
[12] Z. Zhao, X. Yang, W. Cai, Z. Lei, K. Shimizu, Z. Zhang, M. Utsumi, D.-J. Lee, Response of algal-bacterial granular system to low carbon wastewater: focus on granular stability, nutrients removal and accumulation, Bioresour. Technol. 268 (2018) 221–229.
[13] J.S.M. Ahmad, W. Cai, Z. Zhao, Z. Zhang, K. Shimizu, Z. Lei, D.-J. Lee, Stability of algal-bacterial granules in continuous-flow reactors to treat varying strength domestic wastewater, Bioresour. Technol. 244 (2017) 225–233.
[14] Y.-M. Zheng, H.-Q. Yu, S.-J. Liu, X.-Z. Liu, Formation and instability of aerobic granules under high organic loading conditions, Chemosphere 63 (10) (2006) 1791–1800.
[15] B. Long, C.-z Yang, W.-h Pu, J.-k Yang, F.-b Liu, L. Zhang, J. Zhang, K. Cheng, Tolerance to organic loading rate by aerobic granular sludge in a cyclic aerobic granular reactor, Bioresour. Technol. 182 (2015) 314–322.
[16] Ad Mosquera-Corral, M. De Kreuk, J. Heijnen, M. Van Loosdrecht, Effects of oxygen concentration on N-removal in an aerobic granular sludge reactor, Water Res. 39 (12) (2005) 2676–2686.
[17] K.-Y. Show, D.-J. Lee, J.-H. Tay, Aerobic granulation: advances and challenges, Appl. Biochem. Biotechnol. 167 (2012) 1622–1640.
[18] A.S. Abouhend, K. Milferstedt, J. Hamelin, A.A. Ansari, C. Butler, B.I. Carbajal-González, C. Park, Growth progression of oxygenic photogranules and its impact on bioactivity for aeration-free wastewater treatment, Environ. Sci. Technol. 54 (1) (2019) 486–496.
[19] S. Mills, A.C. Trego, P.N. Lens, U.Z. Ijaz, G. Collins, A distinct, flocculent, acidogenic microbial community accompanies methanogenic granules in anaerobic digesters, Microbiol. Spectr. 9 (3) (2021) e00784–21.
[20] J.H. Tay, S.L. Tay, V. Ivanov, S. Pan, H.L. Jiang, Q.S. Liu, Biomass and porosity profiles in microbial granules used for aerobic wastewater treatment, Lett. Appl. Microbiol. 36 (5) (2003) 297–301.
[21] R.D. Franca, H.M. Pinheiro, M.C. van Loosdrecht, N.D. Lourenço, Stability of aerobic granules during long-term bioreactor operation, Biotechnol. Adv. 36 (1) (2018) 228–246.
[22] J. Wang, Z. Li, Z. Lei, X. Qian, Z. Zhang, X. Liu, D.-J. Lee, Disintegration and re-granulation of aged algal-bacterial aerobic granular sludge in wastewater treatment, J. Water Process Eng. 57 (2024) 104614.
[23] B.N. Quoc, M. Armenta, J.A. Carter, R. Bucher, P. Sukapanpotharam, S.J. Bryson, D.A. Stahl, H.D. Stensel, M.-K.H. Winkler, An investigation into the optimal granular sludge size for simultaneous nitrogen and phosphate removal, Water Res. 198 (2021) 117119.
[24] Y.-P. Huang, X. Wang, R.-L. Wang, J.-T. He, Y. Huang, Z.-Y. Hang, X. Chen, Z.-H. Li, Managing stability of aerobic granules by coordinating diameter and denitrification, Sci. Total Environ. 906 (2024) 167795.
[25] K. Torres, F.J. Álvarez-Hornos, P. San-Valero, C. Gabaldón, P. Marzal, Granulation and microbial community dynamics in the chitosan-supplemented anaerobic treatment of wastewater polluted with organic solvents, Water Res. 130 (2018) 376–387.
[26] Y. Zhang, M. Zha, M. Gao, X. Wang, How weak static magnetic field contributes to rapid granulation and better performance of microalgal-bacterial granular sludge? Chem. Eng. J. 450 (2022) 138162.
[27] Z. Wang, W. Chen, J. Wang, M. Gao, D. Zhang, S. Zhang, Y. Hao, H. Song, Exploring the mechanism and negentropy of photogranules for efficient carbon, nitrogen and phosphorus recovery from wastewater, Chem. Eng. J. 476 (2023) 146510.
[28] U. Ullah, A.S. Alkorbid, M. Jalalah, F.A. Harraz, A.I. Alalawy, S.H. Hassan, E.-S. Salama, Lab to large-scale applications of microaeration in anaerobic digestion: biowaste digestibility, microbiome nexus, and reactor stability, J. Environ. Chem. Eng. (2025) 117766.
[29] J. Li, Z. Xiao, J. Gu, Z. Yang, W. Dong, Y. Liu, Z. Xu, W. Zhu, Brewery wastewater as an alternative external carbon source for full-scale municipal wastewater treatment plants: a performance, cost, and environmental assessment, J. Water Process Eng. 72 (2025) 107483.
[30] E.W. Rice, L. Bridgewater, A.P.H. Association, Standard methods for the examination of water and wastewater, American public health association, Washington, DC, 2012.
[31] Y.-W. Lim, S.-A. Lee, S.B. Kim, H.-Y. Yong, S.-H. Yeon, Y.-K. Park, D.-W. Jeong, J.-S. Park, Diversity of denitrifying bacteria isolated from Daejeon sewage treatment plant, J. Microbiol. 43 (5) (2005) 383–390.
[32] X.Y. Li, S.F. Yang, Influence of loosely bound extracellular polymeric substances (EPS) on the flocculation, sedimentation and dewaterability of activated sludge, Water Res. 41 (5) (2007) 1022–1030.
[33] G.L. Peterson, A simplification of the protein assay method of Lowry et al. which is more generally applicable, Anal. Biochem. 83 (2) (1977) 346–356.
[34] M. DuBois, K.A. Gilles, J.K. Hamilton, Pt Rebers, F. Smith, Colorimetric method for determination of sugars and related substances, Anal. Chem. 28 (3) (1956) 350–356.
[35] L. Tang, M. Gao, S. Liang, S. Wang, X. Wang, Enhanced biological phosphorus removal sustained by aeration-free filamentous microalgal-bacterial granular sludge, Water Res. 253 (2024) 121315.
[36] B. Cao, W. Zhang, Y. Du, R. Wang, S.P. Usher, P.J. Scales, D. Wang, Compartmentalization of extracellular polymeric substances (EPS) solubilization and cake microstructure in relation to wastewater sludge dewatering behavior assisted by horizontal electric field: effect of operating conditions, Water Res. 130 (2018) 363–375.
[37] A. Kedves, Z. Kónya, Enhancing granule formation: the role of chitosan and chitosan nanoparticles in microalgal-bacterial granular sludge development, Environ. Technol. Innov. (2025) 104240.
[38] D.B. Sghaier, I. Bankaji, P. Sylvia, I. Caçador, N. Sleimi, Photosynthetic behaviour and mineral nutrition of Tamarix gallica cultivated under aluminum and NaCl combined stress, Phyton 88 (3) (2019) 239.
[39] K. Kitajima, K.P. Hogan, Increases of chlorophyll a/b ratios during acclimation of tropical woody seedlings to nitrogen limitation and high light, Plant Cell Environ. 26 (6) (2003) 857–865.
[40] H.K. Lichtenthaler, [34] Chlorophylls and carotenoids: Pigments of photosynthetic biomembranes, in: in: Methods in enzymology, 148, Elsevier, 1987, pp. 350–382.
[41] L. Zheng, M.-C. Van Labeke, Chrysanthemum morphology, photosynthetic efficiency and antioxidant capacity are differentially modified by light quality, J. Plant Physiol. 213 (2017) 66–74.
[42] V. Pozzobon, N. Cui, A. Moreaud, E. Michiels, W. Levasseur, Nitrate and nitrite as mixed source of nitrogen for Chlorella vulgaris: growth, nitrogen uptake and pigment contents, Bioresour. Technol. 330 (2021) 124995.
[43] W.C. Kuo-Dahab, K. Stauch-White, C.S. Butler, G.J. Gikonyo, B. Carbajal-González, A. Ivanova, S. Dolan, C. Park, Investigation of the fate and dynamics of extracellular polymeric substances (EPS) during sludge-based photogranulation under hydrostatic conditions, Environ. Sci. Technol. 52 (18) (2018) 10462–10471.
[44] M. Basuvaraj, J. Fein, S.N. Liss, Protein and polysaccharide content of tightly and loosely bound extracellular polymeric substances and the development of a granular activated sludge floc, Water Res. 82 (2015) 104–117.
[45] Y. Wang, J. Wang, Z. Liu, X. Huang, F. Fang, J. Guo, P. Yan, Effect of EPS and its forms of aerobic granular sludge on sludge aggregation performance during granulation process based on XDLVO theory, Sci. Total Environ. 795 (2021) 148682.
[46] H.-Q. Yu, Molecular insights into extracellular polymeric substances in activated sludge, Environ. Sci. Technol. 54 (13) (2020) 7742–7750.
[47] X. Wang, T. Chen, C. Gao, Y. Xie, A. Zhang, Use of extracellular polymeric substances as natural redox mediators to enhance denitrification performance by accelerating electron transfer and carbon source metabolism, Bioresour. Technol. 345 (2022) 126522.
[48] M. Kanehisa, S. Goto, KEGG: kyoto encyclopedia of genes and genomes, Nucleic Acids Res. 28 (1) (2000) 27–30.
[49] G. Xie, N.O. Keyhani, C.A. Bonner, R.A. Jensen, Ancient origin of the tryptophan operon and the dynamics of evolutionary change, Microbiol. Mol. Biol. Rev. 67 (3) (2003) 303–342.
[50] L.E. De-Bashan, H. Antoun, Y. Bashan, Involvement of indole-3-acetic acid produced by the growth-promoting bacterium Azospirillum spp. in promoting growth of Chlorella vulgaris 1, J. Phycol. 44 (4) (2008) 938–947.
[51] R. Goss, T. Jakob, Regulation and function of xanthophyll cycle-dependent photoprotection in algae, Photosynth. Res. 106 (1) (2010) 103–122.
[52] A. Pollio, G. Aliotta, G. Pinto, M. Paterno, A. Bevilacqua, Ecophysiological characters and biochemical composition of Stichococcus bacillaris Naegeli strains from low pH environments, Arch. fur Hydrobiol. Suppl. Only 118 (1997) 129–144.
[53] M.Y. Alazaiza, S. He, D. Su, S.S. Abu Amr, P.Y. Toh, M.J. Bashir, Sewage water treatment using Chlorella vulgaris microalgae for simultaneous nutrient separation and biomass production, Separations 10 (4) (2023) 229.
[54] J. Fan, B. Zhang, P.N. Lens, W. Shi, Zero-valent iron enhances nutrient removal and long-term stability of algal-bacterial granular sludge under low carbon conditions, ACS EST Water 4 (8) (2024) 3568–3578.
[55] D. Klimek, M. Herold, M. Calusinska, Comparative genomic analysis of Planctomycetota potential towards complex polysaccharide degradation identifies phylogenetically distinct groups of biotechnologically relevant microbes, bioRxiv (2024), 2024.01. 10.575047.
[56] L. Xie, M. Yang, E. Yang, Z. Liu, X. Geng, H. Chen, Enhanced nitrogen removal by bioelectrochemical coupling anammox and characteristics of microbial communities, Sheng wu Gong. Cheng xue bao= Chin. J. Biotechnol. 39 (7) (2023) 2719–2729.
[57] P. Vico, A. Iriarte, S. Bonilla, C. Piccini, Metagenomic analysis of Raphidiopsisraciborskii microbiome: beyond the individual, Biodivers. Data J. 9 (2021).
[58] J.R. Yordy, T.L. Weaver, Methylobacillus: a new genus of obligately methylotrophic bacteria, Int. J. Syst. Evolut. Microbiol. 27 (3) (1977) 247–255.

[59] C. Martineau, F. Mauffrey, R. Villemur, Comparative analysis of denitrifying activities of Hyphomicrobium nitrativorans, Hyphomicrobium denitrificans, and Hyphomicrobium zavarzinii, Appl. Environ. Microbiol. 81 (15) (2015) 5003–5014.
[60] X. Yang, L. Liu, X. Liu, S. Xie, J. Feng, J. Lv, The responding mechanism of indigenous bacteria in municipal wastewater inoculated with different concentrations of exogenous microalgae, J. Environ. Manag. 345 (2023) 118547.
[61] W. Xiong, S. Wang, Y. Jin, Z. Wu, D. Liu, H. Su, Insights into nitrogen and phosphorus metabolic mechanisms of algal-bacterial aerobic granular sludge via metagenomics: performance, microbial community and functional genes, Bioresour. Technol. 369 (2023) 128442.
[62] L. Jia, B. Jiang, F. Huang, X. Hu, Nitrogen removal mechanism and microbial community changes of bioaugmentation subsurface wastewater infiltration system, Bioresour. Technol. 294 (2019) 122140.
[63] A.R. Fernie, F. Carrari, L.J. Sweetlove, Respiratory metabolism: glycolysis, the TCA cycle and mitochondrial electron transport, Curr. Opin. Plant Biol. 7 (3) (2004) 254–261.
[64] Z. Li, X. Gao, J. Bao, S. Li, X. Wang, Z. Li, L. Zhu, Evaluation of growth and antioxidant responses of freshwater microalgae Chlorella sorokiniana and Scenedesmus dimorphus under exposure of moxifloxacin, Sci. Total Environ. 858 (2023) 159788.
[65] Y. Liu, Z. Liu, F. Wang, Y. Chen, P. Kuschk, X. Wang, Regulation of aerobic granular sludge reformulation after granular sludge broken: effect of poly aluminum chloride (PAC), Bioresour. Technol. 158 (2014) 201–208.
[66] P. Wang, B. Lu, X. Chai, The adaptive regulation mechanism of Anammox granule sludge under calcium ions stress: Defense modes transformation, Water Res. 263 (2024) 122093.
[67] C. Wan, L. Fu, Z. Li, X. Liu, L. Lin, C. Wu, Formation, application, and storage-reactivation of aerobic granular sludge: a review, J. Environ. Manag. 323 (2022) 116302.